tvst

Lacrimal Apparatus, Eyelids, Orbit

Integrated Whole-Exome and Transcriptome Sequencing Indicated Dysregulation of Cholesterol Metabolism in Eyelid Sebaceous Gland Carcinoma

Yuchuan Wang[1–3,*], Jun Li[1–3,*], Peng Hao[1–3,*], Jing Li[1–3], Ruifang Han[1–3], Jinyong Lin[1–3], and Xuan Li[1–3]

[1] Tianjin Eye Hospital, Tianjin Key lab of Ophthalmology and Visual Science, Tianjin Eye Institute, Tianjin, China
[2] Nankai University Affiliated Eye Hospital, Tianjin, China
[3] Clinical College of Ophthalmology, Tianjin Medical University, Tianjin, China

Correspondence: Jun Li and Xuan Li, Tianjin Medical University, 4 Gansu Road, Heping District, Tianjin 300020, China.
e-mails: mike5492@sina.com, xuanli08@yahoo.com

Received: June 21, 2022
Accepted: December 8, 2022
Published: February 3, 2023

Keywords: sebaceous gland carcinoma; sequencing; cholesterol metabolism; SCARB1; PPARG

Citation: Wang Y, Li J, Hao P, Li J, Han R, Lin J, Li X. Integrated whole-exome and transcriptome sequencing indicated dysregulation of cholesterol metabolism in eyelid sebaceous gland carcinoma. Transl Vis Sci Technol. 2023;12(2):4, https://doi.org/10.1167/tvst.12.2.4

Purpose: To identify the molecular background of eyelid sebaceous gland carcinomas (SCs), we conducted the integrated whole-exome sequencing and transcriptome sequencing for eyelid SCs in this study.

Methods: The genetic alterations were studied by whole-exome sequencing, and the messenger RNA expression was studied using Oxford Nanopore Technologies (ONT) in five paired fresh eyelid SC tissues and adjacent normal tissues. Integrated analysis of exome and transcriptomic information was conducted for filtering candidate driver genes. Protein–protein interaction (PPI) network of filtered candidate genes was analyzed by STRING. The protein expression was verified by immunohistochemistry in 29 eyelid SCs and 17 compared normal sebaceous gland tissues.

Results: The average numbers of pathogenic somatic single-nucleotide variants (SNVs) and indels in eyelid SCs were 75 and 28, respectively. Tumor protein p53 (*TP53*), zinc finger protein 750 (*ZNF750*), filaggrin 2 (*FLG2*), valosin-containing protein (*VCP*), and zinc finger protein 717 (*ZNF717*) were recurrent mutated genes. A mean of 844 differentially expressed genes (DEGs) were upregulated, and 1401 DEGs were downregulated in SC samples. The intersection of DEG-based pathways and mutation-based pathways was mainly involved in microbial infection and inflammation, immunodeficiency, cancer, lipid metabolism, and the other pathways. The intersection of DEGs and mutated genes consisted of 55 genes, of which 15 genes formed a PPI network with 4 clusters. The PPI cluster composed of scavenger receptor class B member 1 (SCARB1), peroxisome proliferator–activated receptor γ (PPARG), peroxisome proliferator–activated receptor γ coactivator 1α (PPARGC1A) was involved in cholesterol metabolism. The expression of SCARB1 protein was found to be increased, whereas that of PPARG protein was decreased in eyelid SCs compared to that in the normal sebaceous glands.

Conclusions: Increased SCARB1 and decreased PPARG indicated that dysregulation of cholesterol metabolism might be involved in carcinogenesis of eyelid SCs.

Translational Relevance: The malfunction in cholesterol metabolism might advance our knowledge of the carcinogenesis of eyelid SCs.

Introduction

Sebaceous gland carcinoma (SC) is a rare malignancy with a predilection for eyelid sites but also occurs in extraocular sites. Although rare in the Western Hemisphere, the occurrence of eyelid SC is common in Asian populations, accounting for 33% of eyelid malignancies in China.[1,2] Typical treatment is surgical excision, and recent studies have detailed the efficacy of chemotherapy and radiation.[3] Eyelid SC typically exhibits aggressive local behavior with

recurrence in 18%, metastasis in 8%, and death from metastasis in 6% of eyelid sebaceous cell carcinoma cases.[3] Despite various treatments, effective systemic therapies are lacking, largely because the molecular alterations driving eyelid SC remain poorly understood. To minimize mortality due to eyelid SC, defining the molecular features of eyelid SC to identify the pathways of its pathogenesis and candidates for targeted therapy is critical.

Recently, Tetzlaff et al.[4] applied targeted sequencing in SCs and reported that 52% (14 of 27 cases) harbored somatic mutations in phosphoinositide 3-kinases (PI3K) signaling components. Three extraocular SCs demonstrated a high level of microsatellite instability with somatic mutations in the mismatch-repair genes mutL homolog 1 (*MLH1*) and *MSH2*. However, these mutations of the PI3K pathway and mismatch repair genes are infrequent in Korean eyelid SC.[5] The reason for the above difference might be the difference in race.

A challenge for genomic analysis is to distinguish driver mutations from the complex heterogeneous background landscape of "passenger" somatic alterations, which are not causative factors of oncogenesis. Various tools and strategies have been developed to differentiate driver mutations from passenger alterations. The coanalysis of genomic and transcriptomic data for identification of cancer drivers has helped to elucidate driver mutations and pathways in individual cancers.[6–8]

We hypothesize that genomic alterations with a significant over- or underexpression of genes are high likely to represent cancer drivers. As a proof of concept, we applied this strategy on five paired Chinese eyelid SCs to identify molecular genetic drivers of SC and further evaluated candidate scavenger receptor class B member 1 (SCARB1) and peroxisome proliferator–activated receptor γ (PPARG) in 29 eyelid SCs and 17 compared normal sebaceous glands.

Methods

Study Design

This was a retrospective, clinicopathologic study designed to investigate the molecular background of eyelid SCs. Each tumor was classified according to the American Joint Committee on Cancer (AJCC) eighth edition criteria for eyelid carcinoma.[9] The study was conducted in accordance with the Declaration of Helsinki. With approval from the Medical Ethics Committee of Tianjin Eye Hospital (Number: 2022008), five paired fresh eyelid SCs and adjacent normal tissues; 29 formalin-fixed, paraffin-embedded (FFPE) eyelid SCs; and 17 adjacent normal sebaceous gland tissues were collected. All patients provided written informed consent to obtain tumor biopsies and to perform comprehensive molecular profiling of whole exome, transcriptome, and protein expression. Fresh tissues were frozen in liquid nitrogen. FFPE tissue blocks and hematoxylin and eosin–stained sections of these eyelid SCs were retrieved. Diagnosis was confirmed by two pathologists.

DNA Extraction and Whole-Exome Sequencing

Frozen tissues were extracted using the QIAamp Fast DNA Tissue Kit (Qiagen, Dusseldorf, Germany) for DNA. Extracted DNA was then quantified using Nanodrop. DNA sequencing libraries were captured to exome regions using Agilent SureSelect Human All Exon V6 (Agilent Technologies, Palo Alto, USA). DNA libraries were sequenced to a target depth of $\times 200$ for tumor samples and $\times 100$ for normal samples on the Illumina (San Diego, CA, USA) HiSeq platform.

RNA Extraction and Transcriptome Sequencing

The experimental process was performed according to the standard protocol provided by Oxford Nanopore Technologies (ONT, Oxford, UK), including sample quality detection, library construction, library quality detection, and library sequencing. RNA was subjected to library preparation using the ONT Direct RNA Sequencing Kit. Libraries were sequenced on PromethION. Basecalling was conducted using Guppy (v3.4.3) (ONT) to convert FAST5 into FASTQ files. The full-length sequenced transcriptome was used as a reference for sequence alignment and subsequent analysis, and minimap2 was used to align the clean reads with the reference transcriptome to obtain the corresponding information of the transcript and the reference transcriptome. Fold change ≥ 2 and false discovery rate (FDR) < 0.05 were used as screening criteria for detection of differentially expressed genes (DEGs). Kyoto Encyclopedia of Genes and Genomes (KEGG) pathways were enriched using ClueGO and CluePedia.

Somatic Mutation

For sequencing data, FASTQ files were generated by CASAVA 2.0. The human reference file that was used is GRCh37/hg19. Duplicates were removed using

Picard. The base quality scores were recalibrated using BaseRecalibrator (GATK). Single-nucleotide variations (SNVs) were identified using MuTect. Somatic indels of tumor-normal pairs were called using GATK Somatic Indel Detector. Variant annotations were obtained using the software tool ANNOVAR. Nonsynonymous SNVs, splice site SNVs, stopgain SNVs, and indels of the coding regions were included for further analysis.

Mutational Signature

We used SomaticSignatures to compare our mutational catalog to the previously identified COSMIC mutational signatures (https://cancer.sanger.ac.uk/cosmic/signatures_v2).

Copy Number Variants

The copy number variant (CNV) was identified with Control-FREEC. Frequently mutated CNVs were analyzed using GISTIC.

Germline Mutations of Cancer Predisposing Genes

Germline mutations (SNVs, indels) of normal tissues were called using HaplotypeCaller of GATK. The variants in the Single Nucleotide Polymorphism database (dSNP) or causing synonymous changes were then removed, while the variants in COSMIC were reserved. For the remaining variants, LJB26 (SIFT, PolyPhen, LRT, MutationAssessor, GERP++, PhyloP, SiPhy) was used to identify deleterious variants. Cancer predisposing genes were pooled together from five eyelid SCs, and then the integrated genes were enriched using ClueGO and CluePedia.

Integrative Analysis of Exome and Transcriptome Data and Protein–Protein Interaction Networks

The intersecting DEGs from two or more eyelid SCs were filtered by Venn analysis (http://bioinformatics.psb.ugent.be/webtools/Venn/). The intersecting DEGs and the mutated genes in the union of five eyelid SCs were enriched by ClueGO and CluePedia ($P \leq 0.05$, default settings for KEGG pathway selection). Then the intersection between the DEG-based pathways and the mutation-based pathways was filtered.

The intersecting genes between the DEGs in the union of five eyelid SCs and the mutated genes in the union of five eyelid SCs were used to conduct protein–protein interaction (PPI) networks by STRING (https://cn.string-db.org/) (Fig. 1). Genes involved in PPI networks were more likely to represent cancer drivers.

Immunohistochemistry

FFPE sections of 4 µm thickness were stained with the following immunohistochemistry (IHC) stains: SCARB1 (1:200; Abcam, Cambridge, UK), PPARG (1:300; Abcam, Cambridge, UK), and adipose differentiation-related protein (ADFP) (1:200; Sigma-Aldrich, St. Louis, MO, USA). IHC staining was performed with a Ventana BenchMark GX (Roche Diagnostics). Antigen retrieval was performed by CC1 antigen retrieval solution (Roche Diagnostics) for 30 minutes. Specimens were incubated with primary antibody for 32 minutes, followed by visualization with the ultraView Universal DAB Detection Kit (Roche Diagnostics) for 12 minutes. Sections were counterstained with hematoxylin, dehydrated, and coverslipped. ADFP is the structural component of lipid droplets, which is required for the formation

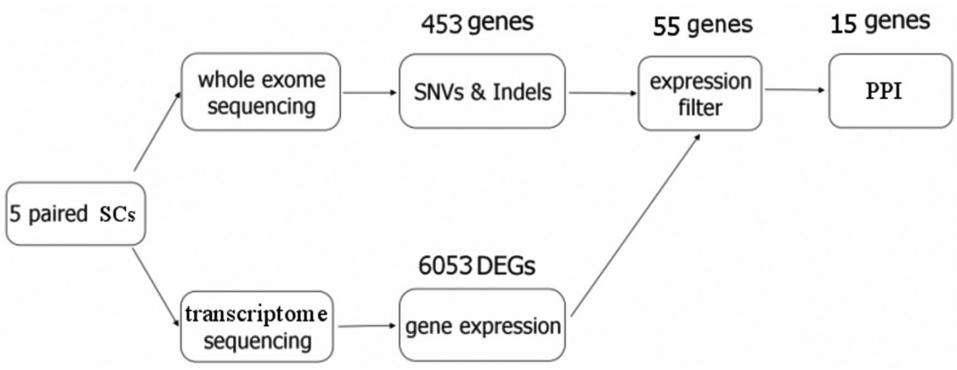

Figure 1. The schema showing the steps of our integrated analysis and filtering procedures. Step 1: The whole exome and transcriptome sequencing were performed for five eyelid SCs. Step 2: The mutated genes or the DEGs were pooled together from five eyelid SCs. Step 3: The intersecting genes between the mutated genes and the DEGs were filtered by Venn analysis. Step 4: The PPI network was built from the intersecting genes using STRING.

and maintenance of lipid storage droplets.[10] ADFP immunostaining is helpful in distinguishing sebaceous carcinoma from other neoplasms with overlapping histology.[11] Interpretation of SCARB1 staining was done by semiquantitative scoring as follows: negative (0) = 0% to 1% of cells positive, weak (1) = 1% to 25% of cells positive, moderate (2) = 26% to 50% of cells positive, and strong (3) = 51% to 100% of cells positive.[12] Interpretation of PPARG staining was done by semiquantitative scoring as follows: negative (0), weak (1), moderate (2), and strong (3).[13]

Statistical Analysis

Data were analyzed with the SPSS statistical package 21.0 (IBM Corp., Armonk, NY, USA). Comparison between variables was performed using the Mann–Whitney *U* rank test. All statistical tests were two-sided, and a *P* value of 0.05 or less was considered statistically significant.

Results

Clinical Characteristics of Eyelid SCs

Of eyelid SCs, 82.3% were located on the upper eyelid. The male to female ratio was 1:2.6. The mean age at diagnosis was 64.1 years. The median follow-up time was 57.5 months (range, 6–103 months), and no patient died of eyelid SC. There were 13 well-differentiated SCs, 9 moderately differentiated SCs, and 7 poorly differentiated SCs. The AJCC eighth edition TNM designations during follow-up were as follows: T1bN0M0, 10; T1cN0M0, 3; T2bN1M0, 9; T2cN0M0, 2; T2cN1M0, 1; T3bN0M0, 1; T3cN1M0, 1; T4aN0M0, 1; and T4bN1M1, 1.

Somatic Mutations and Mutational Signature

The average numbers of pathogenic somatic SNVs and indels in eyelid SCs were 75 and 28, respectively (Fig. 2A; a full list of all SNVs and indels is provided in Supplementary Table S1). *TP53*, *ZNF750*, *FLG2*, *VCP*, and *ZNF717* mutations were recurrent (Supplementary Table S2).

Four samples (4/5) with *ZNF750* mutations showed a mutational signature associated with normal aging, while one sample (1/5) without a *ZNF750* mutation showed an ultraviolet damage signature (Supplementary Table S3).

CNVs

CNVs that were significantly mutated had gains of 1q42.13, 2q37.3, 11p15.5, 11q13.2, and 15q26.3 and losses of 6p22.1, 7q35, 8p11.22, 8q12.1, 19p13.3, 19q13.42, 20q11.21, and 22q13.33 (Fig. 3).

Germline Variants in Cancer Predisposing Genes

In the exome, samples contained a mean of 11 pathogenic germline variants (Supplementary Table S4). Pathogenic germline variants in protein patched homolog 1 (*PTCH1*); protocadherin fat 1 (*FAT1*); breast cancer type 1 susceptibility protein (*BRCA1*); hepatocyte nuclear factor 1α (*HNF1A*); kinase insert domain receptor (*KDR*); PMS1 homolog 2 (*PMS2*); ERCC excision repair 5, endonuclease (*ERCC5*); serine/threonine kinase 11 (*STK11*); and BRCA1-associated RING domain protein 1 (*BARD1*) were recurrent. There were 14 cancer predisposing genes in the union of five eyelid SCs. The enriched cancer predisposing genes were *BARD1*; *BRCA1*; breast cancer type 2 susceptibility protein (*BRCA2*); ERCC

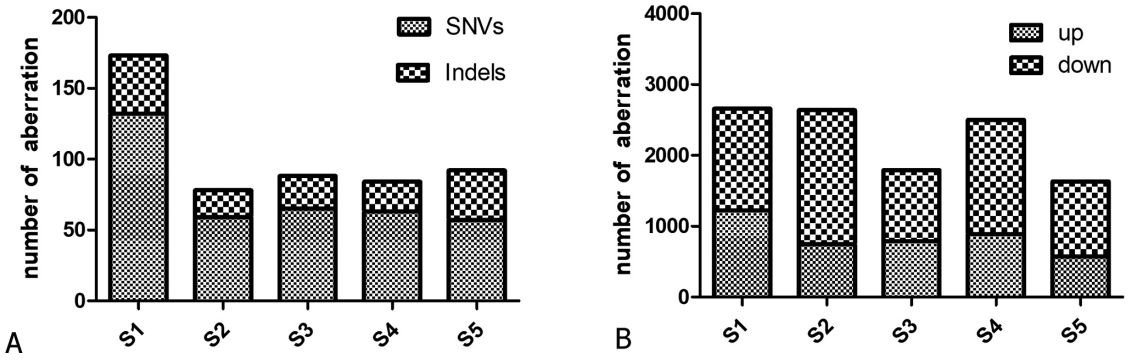

Figure 2. The number of somatic mutations and DEGs in eyelid SCs. (A) The number of somatic mutations, including SNVs and indels. (B) The number of DEGs, including upregulated and downregulated DEGs.

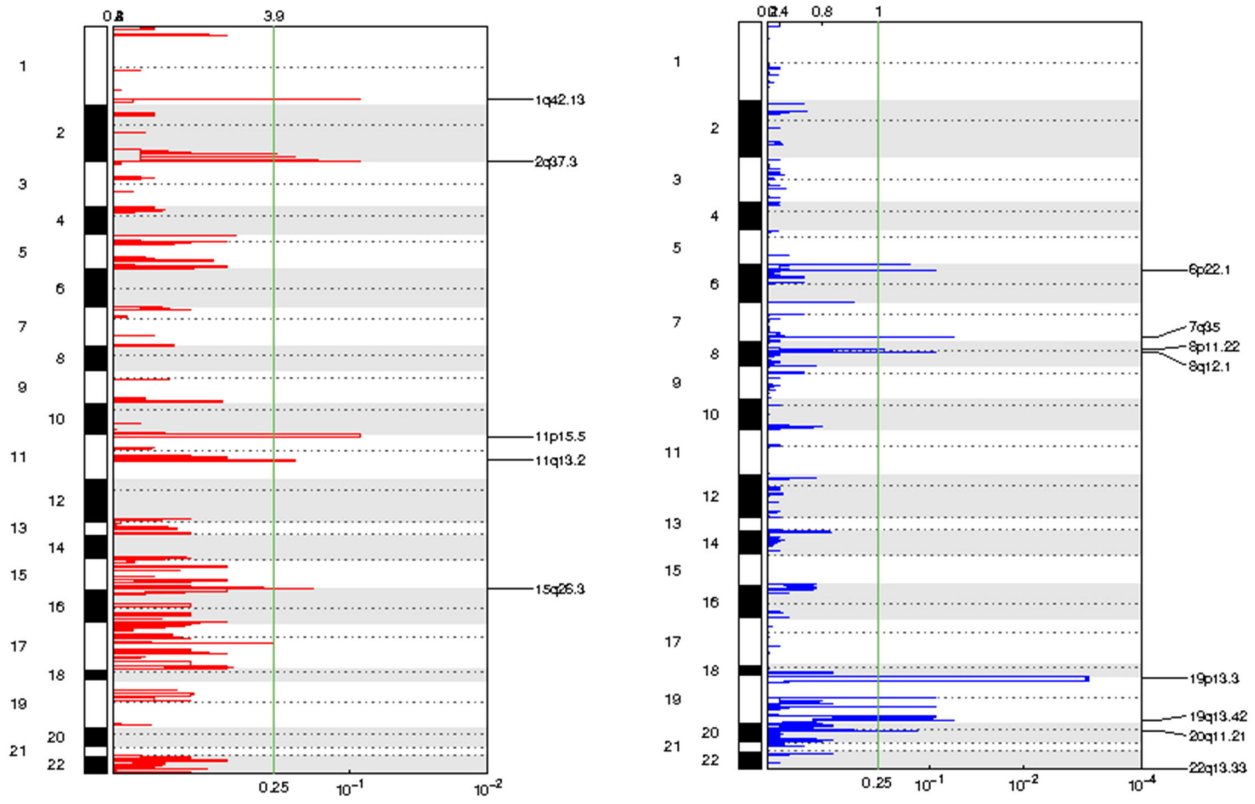

Figure 3. CNVs that are significantly mutated in eyelid SCs. Chromosomal regions with gained (*red*) and lost (*blue*) CNVs identified in five eyelid SCs using GISTIC.

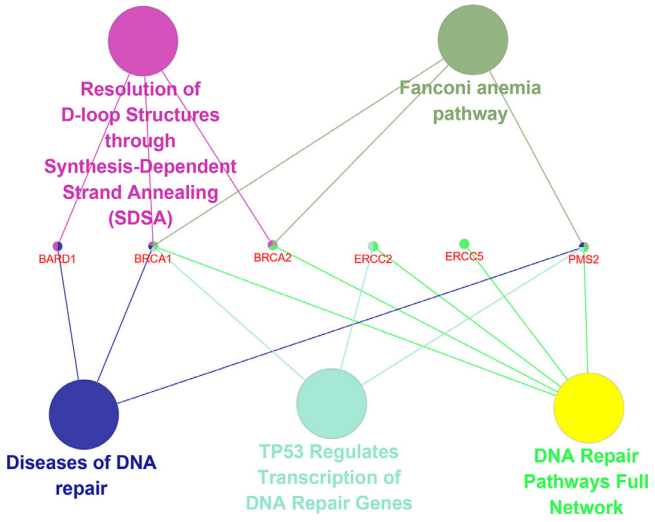

Figure 4. Cancer predisposing genes in eyelid SCs were mainly involved in DNA repair. The *larger circle* represents the pathway, and the *smaller circle* represents the cancer predisposing genes. Pathway analysis was performed using ClueGO and CluePedia. BARD1, BRCA1, BRCA2, ERCC2, ERCC5, and PMS2.

excision repair 2, endonuclease (*ERCC2*); *ERCC5*; and *PMS2*, which were mainly involved in DNA repairs (Fig. 4).

Gene Expression Signature and Pathway Enrichment

There were 6053 DEGs in the union of five eyelid SCs. The average numbers of upregulated DEGs and downregulated DEGs were 844 and 1401 in each eyelid SC sample, respectively (Fig. 2B, Supplementary Table S5). Upregulated DEGs were enriched mainly in the phosphatidylinositol 3-kinase-AKT serine/threonine kinase 1 (PI3K-Akt) signaling pathway, human papillomavirus (HPV) infection, and focal adhesion. Downregulated DEGs were enriched mainly in cytokine–cytokine receptor interaction, PI3K-Akt signaling pathway, and HPV infection.

Integrative Analysis of Exome and Transcriptome Data

There were 2545 DEGs in the intersection of two or more eyelid SCs and 453 mutated genes in the union of five eyelid SCs. Pathway enrichment was performed by using the 2545 DEGs and 453 mutated genes. These genes were associated with 47 representative pathways ($P \leq 0.05$). The intersection between the DEG-based pathways and the mutation-based

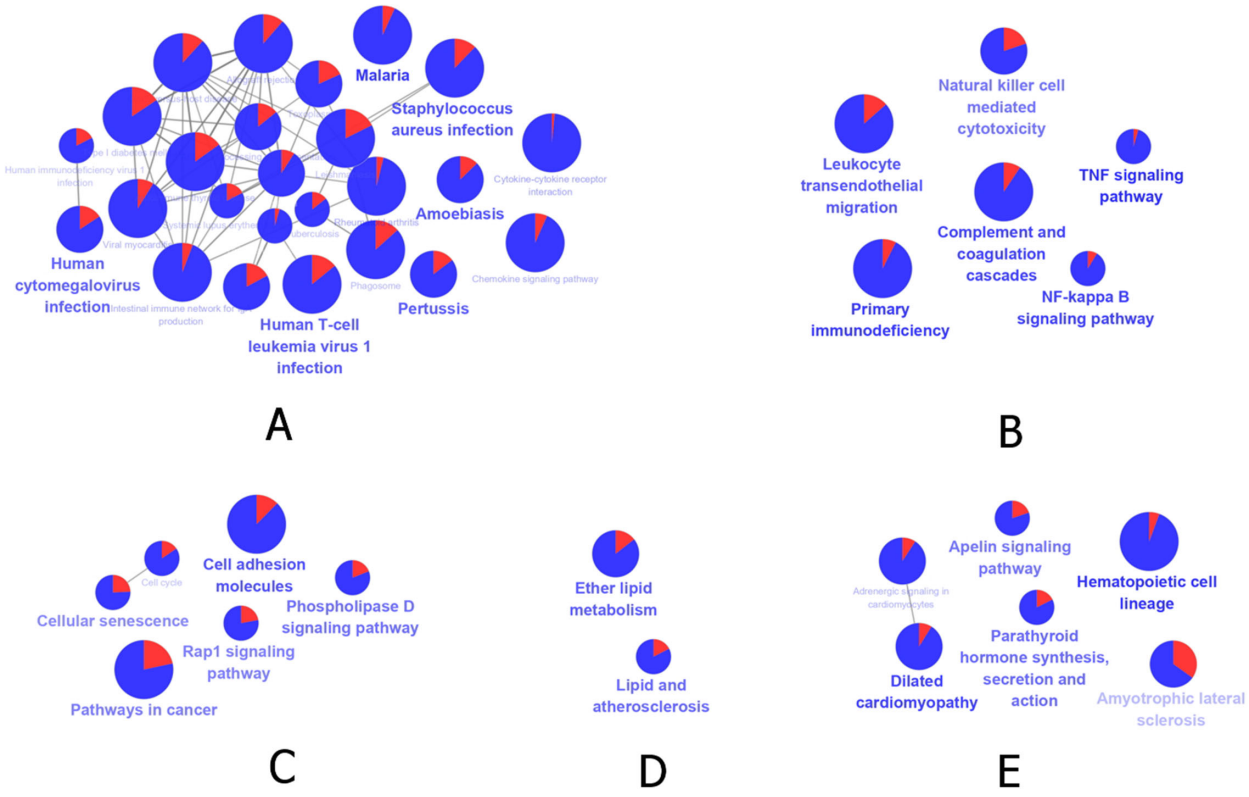

Figure 5. The intersection of the KEGG pathways between exome and transcriptome in eyelid SCs. (A) Pathways in microbial infection and inflammation. (B) Pathways in immunodeficiency. (C) Pathways in cancer. (D) Pathways in lipid metabolism. (E) The other pathways. The *circle* represents the enriched pathway. *Red sector* shows the percentage of mutated genes in the exome; *blue sector* shows the percentage of DEGs in the transcriptome. KEGG pathway enrichment and integrated analysis were performed by ClueGO and CluePedia.

pathways was mainly involved in microbial infection and inflammation, immunodeficiency, cancer, lipid metabolism, and the other pathways (Fig. 5).

There were 453 mutated genes and 6053 DEGs in the union of five eyelid SCs. The intersection between the mutated genes and DEGs consisted of 55 genes, of which 15 genes formed a PPI network. There were four clusters in the PPI network (Fig. 6, Table 1).

Cluster 1 was involved in innate and adaptive immune responses, composed of high-affinity immunoglobulin γ Fc receptor I (FCGR1A); low-affinity immunoglobulin γ Fc region receptor III-A (FCGR3A); HLA class I histocompatibility antigen, B-7α chain (HLA-B); sialic acid–binding Ig-like lectin 9 (SIGLEC9); and WD repeat- and FYVE domain-containing protein 4 (WDFY4).[14–18]

Cluster 2 was involved in cellular proliferation and differentiation, composed of androgen receptor (AR); probable JmjC domain-containing histone demethylation protein 2C (JMJD1C); keratin, type I cytoskeletal 18 (KRT18); and neurogenic locus notch homolog protein 1 (NOTCH1).[19–22]

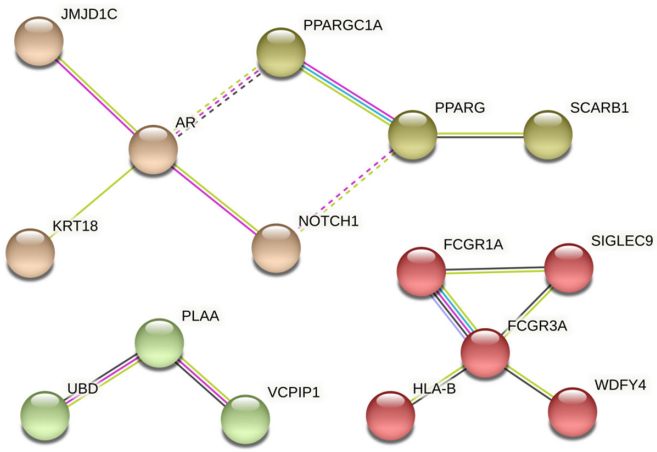

Figure 6. PPI network of filtered genes by integrated exome and transcriptome sequencing. Network nodes represent proteins coded by genes. Edges represent protein–protein associations. The network was clustered to a specified "Markov cluster algorithm inflation parameter" by using STRING. Cluster 1 (*red*): FCGR1A, FCGR3A, HLA-B, SIGLEC9, and WDFY4. Cluster 2 (*brown*): AR, JMJD1C, KRT18, and NOTCH1. Cluster 3 (*yellow*): SCARB1, PPARG, and PPARGC1A. Cluster 4 (*green*): PLAA, UBD, and VCPIP1.

Table 1. Filtered Genes by Integrative Analysis of Exome and Transcriptome Data and PPI Network Analysis

	S1		S2		S3		S4		S5	
Gene	Mutation	mRNA Expression	Mutation	mRNA Expression	Mutation	mRNA Expression	Mutation	mRNA Expression	Mutation	mRNA Expression
SCARB1	Frameshift insertion	Up[a]	—	Up	—	Up	—	Up[a]	—	Up[a]
PPARG	—	Up[a]	—	Down	—	Down	Frameshift insertion	Down[a]	—	Down
AR	—	Up[a]	Nonframeshift deletion	Up	Nonsynonymous SNV	Down[a]	—	Up	—	Down
NOTCH1	—	Down	—	Up	—	Down	Nonsynonymous SNV	Up[a]	—	Down
PPARGC1A	—	Up	—	Up	—	Down	—	Down	Frameshift insertion	Up[a]
JMJD1C	Nonsynonymous SNV	Down[a]	—	Up	—	Down	—	Down	—	Up
KRT18	—	Up[a]	—	Up	—	Up	—	Up[a]	Nonframeshift deletion	Up[a]
FCGR1A	—	Down[a]	—	Down[a]	Stopgain	Up[a]	—	Down	—	Up
FCGR3A	—	Down[a]	—	Down	Nonsynonymous SNV	Up[a]	—	Down	—	Down
HLA-B	Nonsynonymous SNV	Down[a]	—	Down[a]	—	Down	—	Down[a]	—	Down[a]
SIGLEC9	Nonsynonymous SNV	Down[a]	—	Down	—	Up	—	Down	—	Down
WDFY4	—	Down[a]	—	Down[a]	—	Down	Nonsynonymous SNV	Down[a]	—	Down
PLAA	—	Up	Stopgain	Up[a]	—	Up	—	Up	—	Down
UBD	—	Up[a]	—	Down[a]	—	Up	Nonsynonymous SNV	Down[a]	—	Down
VCPIP1	Nonsynonymous SNV	Down[a]	—	Up	—	Up	—	Up	—	Down

—, no mutation.

[a]Fold change ≥ 2 and FDR < 0.05 were used as screening criteria for detection of differentially expressed genes.

Table 2. Protein Expression of SCARB1 and PPARG

Gene	Normal Sebaceous Gland[a]	Sebaceous Gland Carcinoma[a]				*P* Value
		Moderate- to Well-Differentiated Type[b]	Poorly Differentiated Type[b]	T1[c]	T2, T3, and T4[c]	
SCARB1						<0.05,[a] <0.05,[b] >0.05[c]
Negative (0)	0	0	0	0	0	
Weak (1)	17	5	5	3	7	
Moderate (2)	0	4	1	4	1	
Strong (3)	0	13	1	6	8	
PPARG						<0.05,[a] >0.05,[b] >0.05[c]
Negative (0)	0	0	0	0	0	
Weak (1)	0	3	1	2	2	
Moderate (2)	4	16	4	9	11	
Strong (3)	13	3	2	2	3	

[a] *P* value between eyelid normal sebaceous glands and SCs.
[b] *P* value between moderate- to well-differentiated type SCs and poorly differentiated type SCs.
[c] *P* value between T1 stage and T2, T3, and T4 stages.

Cluster 3 was involved in cholesterol metabolism, composed of SCARB1, PPARG, and peroxisome proliferator–activated receptor γ coactivator 1α (PPARGC1A).[23–25]

Cluster 4 was involved in protein ubiquitination, sorting, and degradation, composed of phospholipase A-2–activating protein (PLAA), ubiquitin D (UBD), and deubiquitinating protein VCIP135 (VCPIP1).[26–28]

IHC

ADFP was positive in lipid droplets of the normal immature sebaceous gland cells and SC cells.

The expression of SCARB1 in eyelid SCs was higher than that in normal sebaceous glands ($P < 0.05$). The expression of PPARG in eyelid SCs was lower than that in normal sebaceous glands ($P < 0.05$) (Table 2, Fig. 7).

There were 22 cases in the moderate- to well-differentiated group (moderate-differentiated type, 9; well-differentiated type, 13) and 7 cases in the poorly differentiated group. The expression of SCARB1 in moderate- to well-differentiated group was higher than that in poorly differentiated group ($P < 0.05$). The difference of PPARG expression between the moderate- to well-differentiated group and the poorly differentiated group was not statistically significant ($P > 0.05$) (Table 2).

The difference of SCARB1 or PPARG protein expression between T1 stage and $\geqq$T2 stage was not statistically significant ($P > 0.05$, $P > 0.05$) (Table 2). Because there were too few cases of lymph node and distant metastasis in this group, the relationship between SCARB1, PPARG, and NM stage could not be determined.

Discussion

In this study, we filtered candidate driver genes by integrating whole-exome and transcriptome sequencing data of eyelid SCs. We found that several genes that both mutated and expressed differentially in eyelid SCs were involved in cholesterol metabolism. Our preliminary study indicated that genes, messenger RNAs (mRNAs), and proteins of SCARB1 and PPARG were altered in eyelid SCs.

The integrating exome and transcriptome data indicated the altered pathways in microbial infection and inflammation, immunodeficiency, cancer, lipid metabolism, and the others.

Microbial infection, especially viral infection, is contradictory in SCs. Hayashi et al.[29] first identified HPV in SCs (62%, 9/13) by DNA in situ

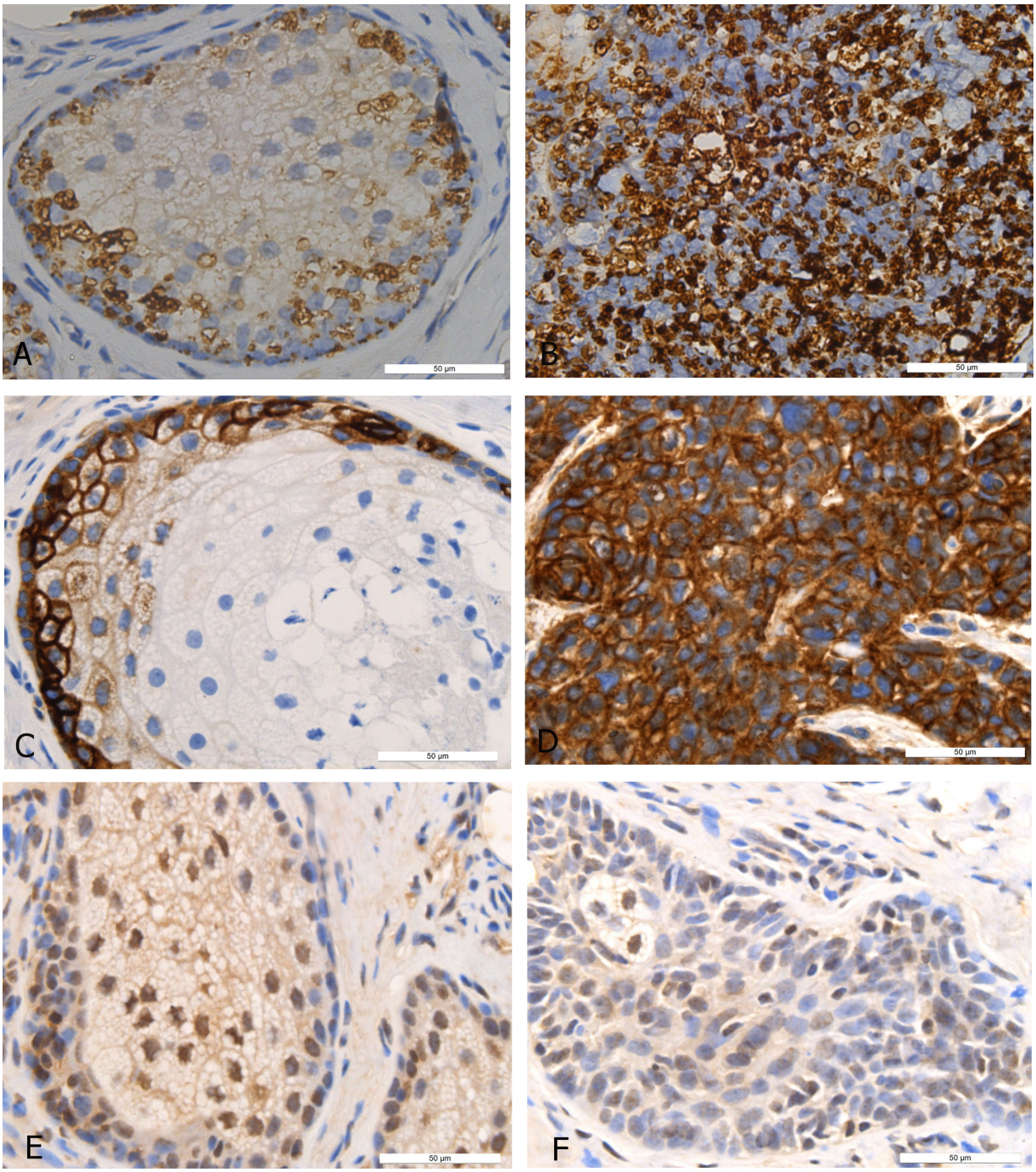

Figure 7. The protein expression of SCARB1 and PPARG in eyelid SCs (IHC, 400×). *Bar*: 50 µm. (A, C, E) Normal sebaceous gland tissues. (B, D, F) Eyelid SCs. (A) ADFP was positive in lipid droplets of the immature sebaceous gland cells. (B) ADFP was positive in lipid droplets of eyelid SCs. (C) SCARB1 was positive in the immature sebaceous gland cells. (D) SCARB1 increased in eyelid SCs. (E) PPARG was positive in the normal sebaceous gland cells. (F) PPARG decreased in eyelid SCs.

hybridization (ISH). However, a subsequent study failed to identify HPV in SCs (0/24) by mRNA ISH.[30] Epstein–Barr virus and Merkel cell polyomavirus were also reported in a part of SCs.[31,32] Recently, immunosuppression has been identified as a strong risk factor for SCs. Among individuals with AIDS and transplant recipients, highly elevated risk (8-fold, 25-fold) for SCs was found.[33,34] We also found the enriched pathways in cancer, cell cycle, cellular senescence, cell adhesion molecules, phospholipase D signaling pathway, and Rap1 signaling pathway, which contribute to carcinogenesis.[35,36]

Interestingly, pathways in lipid metabolism were enriched in eyelid SCs in our study. Hirano and colleagues[37] performed a RNA-sequencing analysis for four eyelid SCs, and the most biological functions that were significantly enriched in the differentially expressed microRNAs and mRNAs were related to lipid metabolism, cell survival, and proliferation. The expression of lipid synthesis and processing proteins adipophilin, ABHD5, and PGRMC1 also indicated the importance of lipid metabolism in SCs.[11,38] Our study and other studies indicated that lipid metabolism might be involved in eyelid SCs.

Cancer has often been coupled with modifications in lipid metabolism, in particular, in cholesterol metabolism.[39] Alterations in cholesterol metabolism have been identified in several cancers.[40] In our study, *SCARB1* and *PPARG* were mutated and dysregulated in eyelid SCs.

SCARB1 is the receptor for different ligands such as phospholipids, cholesterol ester, lipoproteins, phosphatidylserine, and apoptotic cells.[23,41,42] It plays an important role in the regulation of selective uptake of cholesteryl ether and the cholesterol efflux between plasma membrane and high-density lipoprotein (HDL).[43] SCARB1 is an 82-kDa glycoprotein with two transmembrane domains separated by a large extracellular loop.[44] The Cys384 residue of the SCARB1 extracellular loop contributes to the uptake of cholesteryl ester from HDL.[45] The C-terminal domain of SCARB1 interacts with PDZ domain containing 1, which can activate PI3K pathways to promote proliferation and migration.[46]

We preliminarily confirmed that SCARB1 protein was overexpressed in eyelid SCs, and the moderate- to well-differentiated SCs expressed more SCARB1 protein, which might reflect more cholesterol accumulation in highly differentiated eyelid SCs. However, SCARB1 expression was not associated with the Gleason grade of prostate cancer.[47] An elevated SCARB1 expression level has been demonstrated in diverse cancer cell lines and patient tumor samples and correlates with worse patient survival.[48] Upregulation of SCARB1 is required for steroidogenic and nonsteroidogenic cholesterol metabolism in prostate cancer, implicating SCARB1 as a potentially actionable target in prostate cancer.[49] Disrupting SCARB1 function by genetic or chemical inhibitors may decrease clear cell renal cell carcinoma cell malignancy.[50] The main mechanisms of action proposed for these therapeutic interventions are the reduced availability of cholesterol and the decreased activation of the PI3K-AKT pathway.[50] Whether SCARB1 might be a potential molecular pharmacologic target for eyelid SCs needs further investigation.

PPARG is a nuclear receptor that binds peroxisome proliferators such as hypolipidemic drugs and fatty acids.[51] It controls the peroxisomal β-oxidation pathway of fatty acids, playing a key regulator of adipocyte differentiation and glucose homeostasis.[52] PPARG also appears to be a strong regulator of cholesterol homeostasis. PPARG activators induce expression of the gene encoding ATP-binding cassette-transporter A1 (ABCA1), which is involved in apolipoprotein AI–mediated cholesterol efflux from macrophages.[24] Luteinizing hormone/chorionic gonadotropin on the primate preovulatory follicle might reduce the expression of PPARG, resulting in reduced nuclear receptor subfamily 1 group H member 3, with the consequence shifting the balance from cholesterol efflux via ABCA1 and ABCG1 to cholesterol uptake via SCARB1.[53]

In our study, PPARG protein was down-expressed in eyelid SCs. The role of PPARG in tumorigenesis is controversial. A large body of evidence suggests that PPARG functions as a tumor suppressor, as activation of the PPARG/RXRa signaling pathway in different types of cancers leads to the inhibition of cell growth, decreased tumor invasion, and reduced production of proinflammatory cytokines.[54] PPARG regulates multiple aspects of skin physiology, including sebocyte differentiation.[55–57] PPARG-null mouse-preserving PPARG expression in the placenta exhibits total lipoatrophy and complete absence of sebaceous glands.[56] PPARG is present in normal and hyperplastic sebaceous glands, whereas its expression levels are decreased in human sebaceous gland adenoma and human SC cells, reflecting a maturation-linked expression pattern.[57] We also found decreased PPARG expression in eyelid SCs but failed to confirm that PPARG was associated with the degree of tumor differentiation, which may be related to the insufficient number of sample cases in our study.

PPI networks in our study indicated the potential interactions of PPARG–SCARB1, PPARGC1A–PPARG, and NOTCH1–PPARG in eyelid SCs. Other studies have shown that SCARB1 transcription was regulated by PPARG, while PPARGC1A and NOTCH1 were upstream regulatory factors of PPARG. Activation of PPARG promotes transcription of SCARB1 in monocytes, differentiated macrophages, and atherosclerotic lesions of apoE-null mice.[58] PPARGC1A is a transcriptional coactivator for steroid receptors and nuclear receptors. It greatly increases the transcriptional activity of PPARG, which is involved in glucose and fatty acid metabolism.[25] The crosstalk between NOTCH1 and PPARG has also been reported. In 3T3-L1 cells, a preadipocyte cell line, NOTCH1 upregulates PPARG.[59] NOTCH1

intracellular domain-overexpressing Tohoku Hospital Pediatrics 1 cells exhibited increased CD36 levels via activation of PPARG, resulting in enhanced intracellular lipid accumulation.[60]

A limitation of this study is that the number of samples for the integrated analysis of whole-exome and transcriptome sequencing was small, although the filtered genes were subsequently verified in additional *FFPE* samples. We will continue to collect more eyelid SCs for research in the future. In addition, further in vitro and in vivo studies are required to elucidate the mechanism of SCARB1 and PPARG involved in cholesterol metabolism in eyelid SC carcinogenesis.

Data Availability

RNA sequence data have been deposited in NCBI's Gene Expression Omnibus (GEO) and are accessible through GEO Series accession number GSE219205. The links of DNA sequence data to NCBI's Sequence Read Archive (SRA) database appear on the GEO records. For information on GEO linking and citing, please refer to https://www.ncbi.nlm.nih.gov/geo/info/linking.html.

Acknowledgments

Supported by grants from the National Natural Science Foundation of China (82171024), the Tianjin Science & Technology Foundation (20JCYBJC01450, 15JCZDJC35300), the Science and Technology Fund Project of Tianjin Eye Hospital (YKQN2005), and Tianjin Key Medical Discipline (Specialty) Construction Project.

Disclosure: **Y. Wang**, None; **J. Li**, None; **P. Hao**, None; **J. Li**, None; **R. Han**, None; **J. Lin**, None; **X. Li**, None

* YW, JL, and PH contributed equally to this work.

References

1. Shields JA, Demirci H, Marr BP, et al. Sebaceous carcinoma of the ocular region: a review. *Surv Ophthalmol*. 2005;50(2):103–122.
2. Ni C, Searl SS, Kuo PK, et al. Sebaceous cell carcinomas of the ocular adnexa. *Int Ophthalmol Clin*. 1982;22(1):23–61.
3. Shields JA, Saktanasate J, Lally SE, et al. Sebaceous carcinoma of the ocular region: the 2014 Professor Winifred Mao Lecture. *Asia Pac J Ophthalmol (Phila)*. 2015;4(4):221–227.
4. Tetzlaff MT, Singh RR, Seviour EG, et al. Next-generation sequencing identifies high frequency of mutations in potentially clinically actionable genes in sebaceous carcinoma. *J Pathol*. 2016;240(1):84–95.
5. Kwon MJ, Nam ES, Cho SJ, et al. Mutation analysis of CTNNB1 gene and the ras pathway genes KRAS, NRAS, BRAF, and PIK3CA in eyelid sebaceous carcinomas. *Pathol Res Pract*. 2017;213(6):654–658.
6. Peifer M, Fernández-Cuesta L, Sos ML, et al. Integrative genome analyses identify key somatic driver mutations of small-cell lung cancer. *Nat Genet*. 2012;44(10):1104–1110.
7. Robinson DR, Wu YM, Lonigro RJ, et al. Integrative clinical genomics of metastatic cancer. *Nature*. 2017;548(7667):297–303.
8. Hu Y, Zhang X, Wang O, et al. Integrated whole-exome and transcriptome sequencing of sporadic parathyroid adenoma. *Front Endocrinol (Lausanne)*. 2021;12:631680.
9. Amin MB, Edge SB, Greene FL, et al., eds. *AJCC Cancer Staging Manual*. 8th ed. New York, NY: Springer; 2017.
10. Liu R, Lee JH, Li J, et al. Choline kinase alpha 2 acts as a protein kinase to promote lipolysis of lipid droplets. *Mol Cell*. 2021;81(13):2722–2735.
11. Boussahmain C, Mochel MC, Hoang MP. Perilipin and adipophilin expression in sebaceous carcinoma and mimics. *Hum Pathol*. 2013;44(9):1811–1816.
12. Jiang T, Diao X, Ding M, et al. SR-B1 and CD10 combined immunoprofile for differential diagnosis of metastatic clear cell renal cell carcinoma and clear cell carcinoma of the ovary. *J Mol Histol*. 2021;52(3):539–544.
13. Meyer S, Vogt T, Landthaler M, et al. Cyclooxygenase 2 (COX2) and peroxisome proliferator-activated receptor gamma (PPARG) are stage-dependent prognostic markers of malignant melanoma. *PPAR Res*. 2009;2009:848645.
14. van Vugt MJ, Kleijmeer MJ, Keler T, et al. The FcgammaRIa (CD64) ligand binding chain triggers major histocompatibility complex class II antigen presentation independently of its associated FcR gamma-chain. *Blood*. 1999;94(2):808–817.
15. DiLillo DJ, Tan GS, Palese P, et al. Broadly neutralizing hemagglutinin stalk-specific antibodies require FcγR interactions for protection against influenza virus in vivo. *Nat Med*. 2014;20(2):143–151.

16. Kløverpris HN, Cole DK, Fuller A, et al. A molecular switch in immunodominant HIV-1-specific CD8 T-cell epitopes shapes differential HLA-restricted escape. *Retrovirology*. 2015;12:20.
17. Zheng Y, Ma X, Su D, et al. The roles of Siglec7 and Siglec9 on natural killer cells in virus infection and tumour progression. *J Immunol Res*. 2020;2020:6243819.
18. Theisen DJ, Davidson JT, Briseño CG, et al. WDFY4 is required for cross-presentation in response to viral and tumor antigens. *Science*. 2018;362(6415):694–699.
19. Yang J, Zhao YL, Wu ZQ, et al. The single-macro domain protein LRP16 is an essential cofactor of androgen receptor. *Endocr Relat Cancer*. 2009;16(1):139–153.
20. Schimek V, Björn N, Pellé L, et al. JMJD1C knockdown affects myeloid cell lines proliferation, viability, and gemcitabine/carboplatin-sensitivity. *Pharmacogenet Genomics*. 2021;31(3):60–67.
21. Chen B, Xu X, Lin DD, et al. KRT18 modulates alternative splicing of genes involved in proliferation and apoptosis processes in both gastric cancer cells and clinical samples. *Front Genet*. 2021;12:635429.
22. Brütsch R, Liebler SS, Wüstehube J, et al. Integrin cytoplasmic domain-associated protein-1 attenuates sprouting angiogenesis. *Circ Res*. 2010;107(5):592–601.
23. Trigatti B, Rigotti A, Krieger M. The role of the high-density lipoprotein receptor SR-BI in cholesterol metabolism. *Curr Opin Lipidol*. 2000;11(2):123–131.
24. Chinetti G, Lestavel S, Bocher V, et al. PPAR-alpha and PPAR-gamma activators induce cholesterol removal from human macrophage foam cells through stimulation of the ABCA1 pathway. *Nat Med*. 2001;7(1):53–58.
25. Knutti D, Kaul A, Kralli A. A tissue-specific coactivator of steroid receptors, identified in a functional genetic screen. *Mol Cell Biol*. 2000;20(7):2411–2422.
26. Papadopoulos C, Kirchner P, Bug M, et al. VCP/p97 cooperates with YOD1, UBXD1 and PLAA to drive clearance of ruptured lysosomes by autophagy. *EMBO J* 2017;36(2):135–150.
27. Hipp MS, Kalveram B, Raasi S, et al. FAT10, a ubiquitin-independent signal for proteasomal degradation. *Mol Cell Biol*. 2005;25(9):3483–3491.
28. Huang J, Zhou Q, Gao M, et al. Tandem deubiquitination and acetylation of SPRTN promotes DNA-protein crosslink repair and protects against aging. *Mol Cell*. 2020;79(5):824–835.e5.
29. Hayashi N, Furihata M, Ohtsuki Y, et al. Search for accumulation of p53 protein and detection of human papillomavirus genomes in sebaceous gland carcinoma of the eyelid. *Virchows Arch*. 1994;424(5):503–509.
30. Stagner AM, Afrogheh AH, Jakobiec FA, et al. p16 expression is not a surrogate marker for high-risk human papillomavirus infection in periocular sebaceous carcinoma. *Am J Ophthalmol*. 2016;170:168–175.
31. Tanahashi J, Kashima K, Daa T, et al. Merkel cell carcinoma co-existent with sebaceous carcinoma of the eyelid. *J Cutan Pathol*. 2009;36(9):983–986.
32. Gao H, Tang L, Lin J, et al. Detection of Epstein-Barr virus in 130 cases of eyelid sebaceous gland carcinoma using in situ hybridization. *J Ophthalmol*. 2020;2020:7354275.
33. Lanoy E, Dores GM, Madeleine MM, et al. Epidemiology of nonkeratinocytic skin cancers among persons with AIDS in the United States. *AIDS*. 2009;23(3):385–393.
34. Sargen MR, Cahoon EK, Lynch CF, et al. Sebaceous carcinoma incidence and survival among solid organ transplant recipients in the United States, 1987–2017. *JAMA Dermatol*. 2020;156(12):1307–1314.
35. Bruntz RC, Lindsley CW, Brown HA. Phospholipase D signaling pathways and phosphatidic acid as therapeutic targets in cancer. *Pharmacol Rev*. 2014;66(4):1033–1079.
36. Hattori M, Minato N. Rap1 GTPase: functions, regulation, and malignancy. *J Biochem*. 2003;134(4):479–484.
37. Hirano T, Yunoki T, Furusawa Y, et al. Bioinformatics analysis of the microRNA-mRNA network in sebaceous gland carcinoma of the eyelid. *Mol Med Rep*. 2021;23(1):44.
38. Chen WS, Chen PL, Li J, et al. Lipid synthesis and processing proteins ABHD5, PGRMC1 and squalene synthase can serve as novel immunohistochemical markers for sebaceous neoplasms and differentiate sebaceous carcinoma from sebaceoma and basal cell carcinoma with clear cell features. *J Cutan Pathol*. 2013;40(7):631–638.
39. Kuzu OF, Noory MA, Robertson GP. The role of cholesterol in cancer. *Cancer Res*. 2016;76(8):2063–2070.
40. Vona R, Iessi E, Matarrese P. Role of cholesterol and lipid rafts in cancer signaling: a promising therapeutic opportunity? *Front Cell Dev Biol*. 2021;9:622908.
41. Kawasaki Y, Nakagawa A, Nagaosa K, et al. Phosphatidylserine binding of class B scavenger

receptor type I, a phagocytosis receptor of testicular Sertoli cells. *J Biol Chem*. 2002;277(30):27559–27566.
42. Vergeer M, Korporaal SJ, Franssen R, et al. Genetic variant of the scavenger receptor BI in humans. *N Engl J Med*. 2011;364(2):136–145.
43. Zanoni P, Khetarpal SA, Larach DB, et al. Rare variant in scavenger receptor BI raises HDL cholesterol and increases risk of coronary heart disease. *Science*. 2016;351(6278):1166–1171.
44. Acton SL, Scherer PE, Lodish HF, et al. Expression cloning of SR-BI, a CD36-related class B scavenger receptor. *J Biol Chem*. 1994;269(33):21003–21009.
45. Yu M, Romer KA, Nieland TJ, et al. Exoplasmic cysteine Cys384 of the HDL receptor SR-BI is critical for its sensitivity to a small-molecule inhibitor and normal lipid transport activity. *Proc Natl Acad Sci USA*. 2011;108(30):12243–12248.
46. Zhu W, Saddar S, Seetharam D, et al. The scavenger receptor class B type I adaptor protein PDZK1 maintains endothelial monolayer integrity. *Circ Res*. 2008;102(4):480–487.
47. Stopsack KH, Gerke TA, Andrén O, et al. Cholesterol uptake and regulation in high-grade and lethal prostate cancers. *Carcinogenesis*. 2017;38(8):806–811.
48. Vasquez M, Simões I, Consuegra-Fernández M, et al. Exploiting scavenger receptors in cancer immunotherapy: lessons from CD5 and SR-B1. *Eur J Immunol*. 2017;47(7):1108–1118.
49. Gordon JA, Noble JW, Midha A, et al. Upregulation of scavenger receptor B1 Is required for steroidogenic and nonsteroidogenic cholesterol metabolism in prostate cancer. *Cancer Res*. 2019;79(13):3320–3331.
50. Riscal R, Bull CJ, Mesaros C, et al. Cholesterol auxotrophy as a targetable vulnerability in clear cell renal cell carcinoma. *Cancer Discov*. 2021;11(12):3106–3125.
51. Mukherjee R, Jow L, Croston GE, et al. Identification, characterization, and tissue distribution of human peroxisome proliferator-activated receptor (PPAR) isoforms PPARgamma2 versus PPARgamma1 and activation with retinoid X receptor agonists and antagonists. *J Biol Chem*. 1997;272(12):8071–8076.
52. Yin Y, Yuan H, Wang C, et al. 3-phosphoinositide-dependent protein kinase-1 activates the peroxisome proliferator-activated receptor-gamma and promotes adipocyte differentiation. *Mol Endocrinol*. 2006;20(2):268–278.
53. Puttabyatappa M, Vandevoort CA, Chaffin CL. hCG-induced down-regulation of PPARγ and liver X receptors promotes periovulatory progesterone synthesis by macaque granulosa cells. *Endocrinology*. 2010;151(12):5865–5872.
54. Chi T, Wang M, Wang X, et al. PPAR-γ modulators as current and potential cancer treatments. *Front Oncol*. 2021;11:737776.
55. Billoni N, Buan B, Gautier B, et al. Expression of peroxisome proliferator activated receptors (PPARs) in human hair follicles and PPAR alpha involvement in hair growth. *Acta Derm Venereol*. 2000;80(5):329–334.
56. Sardella C, Winkler C, Quignodon L, et al. Delayed hair follicle morphogenesis and hair follicle dystrophy in a lipoatrophy mouse model of Pparg total deletion. *J Invest Dermatol*. 2018;138(3):500–510.
57. Dozsa A, Dezso B, Toth BI, et al. PPARγ-mediated and arachidonic acid-dependent signaling is involved in differentiation and lipid production of human sebocytes. *J Invest Dermatol*. 2014;134(4):910–920.
58. Chinetti G, Gbaguidi FG, Griglio S, et al. CLA-1/SR-BI is expressed in atherosclerotic lesion macrophages and regulated by activators of peroxisome proliferator-activated receptors. *Circulation*. 2000;101(20):2411–2417.
59. Garcés C, Ruiz-Hidalgo MJ, Font de Mora J, et al. Notch-1 controls the expression of fatty acid-activated transcription factors and is required for adipogenesis. *J Biol Chem*. 1997;272(47):29729–29734.
60. Sangphech N, Keawvilai P, Palaga T. Notch signaling increases PPARγ protein stability and enhances lipid uptake through AKT in IL-4-stimulated THP-1 and primary human macrophages. *FEBS Open Bio*. 2020;10(6):1082–1095.